



OPEN

Dynamic peripheral traction forces balance stable neurite tension in regenerating *Aplysia* bag cell neurons

SUBJECT AREAS:
CELLULAR MOTILITY
CELLULAR NEUROSCIENCECallen Hyland¹, Aaron F. Mertz², Paul Forscher¹ & Eric Dufresne^{2,3}Received
17 January 2014Accepted
24 April 2014Published
14 May 2014Correspondence and
requests for materials
should be addressed to
E.R.D. (eric.dufresne@
yale.edu)¹Department of Molecular, Cellular, and Developmental Biology, Yale University, New Haven, CT 06520, ²Department of Physics, Yale University, New Haven, CT 06520, ³Departments of Mechanical Engineering & Materials Science, Chemical & Environmental Engineering, and Cell Biology, Yale University, New Haven, CT 06520.

Growth cones of elongating neurites exert force against the external environment, but little is known about the role of force in outgrowth or its relationship to the mechanical organization of neurons. We used traction force microscopy to examine patterns of force in growth cones of regenerating *Aplysia* bag cell neurons. We find that traction is highest in the peripheral actin-rich domain and internal stress reaches a plateau near the transition between peripheral and central microtubule-rich domains. Integrating stress over the area of the growth cone reveals that total scalar force increases with area but net tension on the neurite does not. Tensions fall within a limited range while a substantial fraction of the total force can be balanced locally within the growth cone. Although traction continuously redistributes during extension and retraction of the peripheral domain, tension is stable over time, suggesting that tension is a tightly regulated property of the neurite independent of growth cone dynamics. We observe that redistribution of traction in the peripheral domain can reorient the end of the neurite shaft. This suggests a role for off-axis force in growth cone turning and neuronal guidance.

Development of the nervous system is a complex series of events that involves large scale tissue morphogenesis and migrations of cells. These events involve mechanical forces, but the mechanical properties of the nervous system are poorly understood compared to its chemical and electrophysiological properties. An exemplary feature of the nervous system is the great distance that neurites must extend from the cell body to their synaptic target¹. At once each neuron must function as a single connected unit and as a set of compartments capable of responding to local stimuli. Abundant evidence indicates that neurites are under tension both *in vitro*^{2–7} and *in vivo*^{8–10}, suggesting one means of cell-scale mechanical integration. The physiological significance of this tension is not fully understood, but several roles have been suggested¹¹. Tension can be a stimulus for growth during growth cone-driven neurite elongation³, neurite towing by moving target cells¹², and the post-synaptogenesis stretch that elongates neurites during organismal growth^{1,13–15}. Tension can also specify axonal identity¹⁶, drive neurite pruning¹⁷ and may contribute to compact wiring of the nervous system^{18,19}.

It follows by simple force balance that growth cones, the dynamic, migrating tips of elongating neurites, must exert traction equal and opposite to neurite tension to resist retraction. Growth cone tractions have been measured using traction force microscopy (TFM) on compliant substrates in several recent studies^{20–25}, however the mechanism of force generation is mostly unknown, as is its role in powering outgrowth. Traction force has been explored extensively in other motile cells types^{26–28}, but growth cones present several unique features and experimental challenges. Growth cones exert much lower forces than other cell types consistent with their adaption to the relatively soft environment of the nervous system. Growth cones are also tethered to the cell body and other growth cones through the neurite shaft and therefore must be considered as a compartment of a much larger structure. The mechanical coupling between the growth cone and the neurite thus becomes crucial for understanding outgrowth.

The growth cone is organized into compartments with distinct cytoskeletal architecture. The peripheral domain (labeled P, Figure 1a) is composed of a highly dynamic network of crosslinked actin filaments^{29–31}. The central domain (labeled C, Figure 1a) contains a parallel array of uncrosslinked microtubules and their organelle cargos as well as stable bundles of actin filaments^{32,33}. In the transition zone (labeled T, Figure 1a), the peripheral actin network condenses into contractile arc structures^{32,33}, which are in turn connected to central domain actin bundles and the contractile actin node in the growth cone neck (labeled N, Figure 1a)^{33,34}.

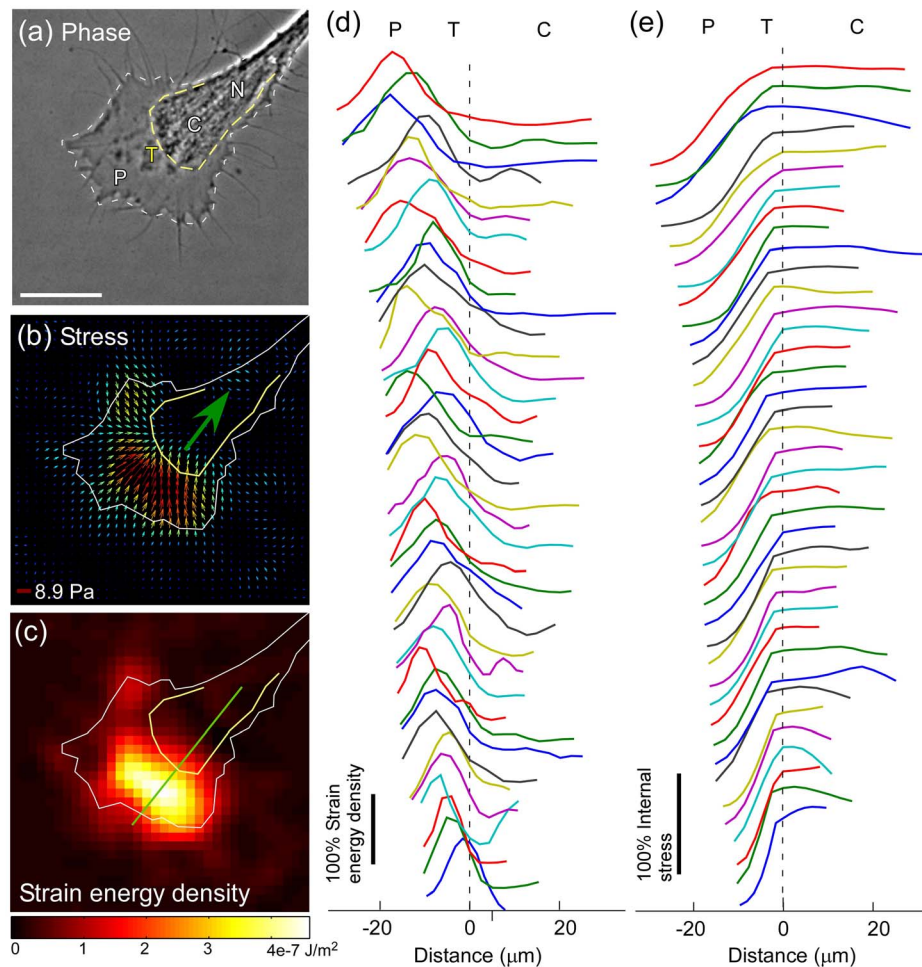


Figure 1 | Spatial distribution of force in growth cones. (a) Representative phase contrast image of *Aplysia* bag cell growth cone. P = peripheral domain, T = transition zone, C = central domain, N = growth cone neck. Scale bar is 20 μm . (b) Map of traction stress vectors in growth cone from (a) showing localization of traction force in peripheral domain. White outline shows edge of growth cone and neurite. (c) Map of strain energy density for growth cone in (a). Green line shows location of linescan. (d) Linescans of strain energy density through 38 growth cones. Traces are shifted such that the boundaries between peripheral and central domains align at zero. For each trace, values are normalized to the maximum value in that trace. (e) Internal stress measured along the same line scans as (d) normalized to maximum value in each trace.

Aplysia californica bag cell neurons have been used extensively to study the cytoskeletal dynamics underlying growth cone behavior on account of their large size and spread morphology. Here we use TFM with soft silicone substrates to explore the spatial and temporal pattern of force during bag cell neurite elongation. We show that neurite shafts are under tension and that tension is balanced by traction force in the growth cone peripheral domain. Growth cones can also exert forces that are balanced in other parts of the growth cone, which account for a variable proportion of total force. Although peripheral force patterns are extremely dynamic the tension is consistent over time. The progression of traction patterns during outgrowth suggests that a constant load continuously redistributes as adhesions are broken and formed. These observations suggest a physical mechanism for neurite turning wherein asymmetry of peripheral traction force reorients the tension and bends the end of the neurite toward regions of higher force.

Results and Discussion

Growth cones generate traction force in the peripheral domain.

The mechanical engagement between growth cones and the extracellular environment drives the elongation of developing and regenerating neurites. Force measurement using compliant substrates was undertaken to extend our knowledge of the role of traction in growth. We have used displacements of tracer beads in

a soft silicone gel to calculate the stress field, a vector map of force per unit area, and strain energy density, a scalar measure of the energy expended by the growth cone to deform the substrate. Figure 1b shows a typical stress distribution and Figure 1c the corresponding strain energy density.

Traction stresses applied by the growth cone on the substrate are centripetal, pointed away from the leading edge and toward the central domain. This follows the direction of flow of the underlying actin cytoskeleton. Actin filaments assemble at the leading edge and disassemble throughout the peripheral domain^{35,36}. The push of leading edge polymerization and pull of myosin motors within the network drives steady centripetal movement called retrograde flow^{35,37,38}. We found that highest stress and strain energy are consistently localized in the peripheral domain (Fig. 1 b,c, Supplementary Fig. S1). The spatial distribution of traction force was examined in 38 growth cones in which the boundary between peripheral and central domains was clear (dashed yellow line, Fig. 1a). Linescans from the leading edge, through the point of highest force, and into the growth cone neck (green line in Fig. 1c) allowed comparison of stress patterns among a large number of growth cones. The linescans confirm that traction is primarily within the peripheral domain, however, the position of the peak of strain energy relative to the leading edge varies greatly between growth cones as does the width of the peripheral domain (Fig. 1b,c,d, Supplementary



Fig. S1). Traction against the substrate must be balanced by internal stress on the cytoskeleton and other intracellular structures. Internal stress can be calculated as the integral of the traction stresses between each point on the line and the leading edge^{39,40}. We find that it rises throughout the peripheral domain, reaches a plateau in the transition zone, and continues at this level into the central domain (Fig. 1e, Supplementary Fig. S1).

Consistent with the localization of traction force to the peripheral domain, cytochalasin B, which caps barbed end polymerization sites at the leading edge³⁵, led to collapse of the peripheral domain and cessation of traction force (Supplementary Fig. S2). The peripheral domain collapse was reversible with drug washout. Jaspilakinolide, which inhibits actin network turnover³⁶, also led to peripheral retraction and inhibited traction force (Supplementary Fig. S2). These results show that continuous assembly and disassembly of the actin network is necessary to maintain peripheral domain traction.

Maximum traction stresses were typically a few Pascal (mean 90th percentile stress 6.8 ± 2.8 Pa), confirming that neurons are among the weakest cell types^{41–44}. We measure maximum internal stresses in the range of a few kilopascal (Supplementary Fig. S1) showing that although growth cone tractions are relatively weak the accumulated levels of cytoskeletal stress might be considerable. These results are generically consistent, but differ in detail, with previous reports of traction force in growth cones. The peripheral domain actin network includes parallel bundles called filopodia and branched meshworks between filopodia called veils^{30,31}. We clearly see the highest force under regions with veils and relatively low force under long filopodia (Fig. 1, Supplementary Fig. S1), contrasting with previous reports that have focused on force generated by individual filopodia extending beyond the veil^{22,23}. While others have shown highest stress at the leading edge^{20,21}, we find variable positioning of peak stress within the peripheral domain (Fig. 1b,c and Supplementary Fig. S1). The pattern of internal stress reported here contrasts with published maps showing converging centripetal and outward directed forces near the transition zone²⁰. We have found that internal force reaches a plateau in the transition zone and does not decrease into the growth cone neck, implying that this force is either balanced in other parts of the growth cone or transmitted to the rest of the cell as tension in the neurite shaft.

Neurite tension is independent of area. Since mechanical equilibrium requires that the vector sum of traction stresses over the entire cell must equal zero, if the vector sum over the area of an individual growth cone is non-zero then this net force must be transmitted to the rest of the cell. We found that vector sums of traction stresses in growth cones give a net force in the direction of the neurite shaft (large green arrow, Fig. 1b), which is equivalent to the tension transmitted to the rest of the cell^{20,21}. The scalar sum of stress over the growth cone area gives the total force that the growth cone is capable of generating. This commonly computed quantity^{44,45} does not have a physical meaning, but when compared to the tension gives insight into the geometry of stresses in the cell. Mean tension was 3.1 ± 1.6 nN, while the mean total force was 6.5 ± 3.8 nN ($n = 117$) (Fig. 2a). The higher variability of total force can be accounted for by the observation that total force scales with growth cone area ($r^2 = 0.55$, blue symbols) while the tension is very weakly correlated with area ($r^2 = 0.14$, red symbols) (Fig. 2c). The increase of total force with size cannot be accounted for by higher stress levels in larger growth cones since the 90th percentile of the stress shows no correlation with size (Fig. 2b). The values of total force are all greater than the values expected if the area contained only background noise (Fig. 1c, green line). The values for tension reported here are consistent with reported values measured both with TFM^{20,21} and other methods^{4–6,10}.

The discrepancy between tension and total force can be understood as a consequence of the geometry of stress vectors in the growth

cone. The ratio of tension to total force (referred to hereafter as the ‘tension ratio’) gives the proportion of the force that is not balanced locally within the growth cone and therefore must be balanced elsewhere in the cell. This quantity is functionally equivalent to the ‘unbalanced traction’ introduced to characterize force at cell-cell junctions^{44,45}. For an isolated cell or compartment, mechanical equilibrium requires zero net force and therefore a tension ratio of zero, whereas if all stress in the growth cone contributed to resisting neurite tension the ratio would be close to one (Fig. 2d). We found that growth cones with low tension ratios often have stresses near the neck partially balancing the rearward-directed stresses in more distal regions (Fig. 2f). While contractile stress associated with the cell margins appears to be a universal feature of adherent cells, such partially isolated contractile compartments have, to our knowledge, never been reported and might be a unique feature of neurons.

Tension ratios for growth cones with area lower than the median (mean 0.6 ± 0.2 , $n = 58$) are significantly higher than tension ratios for growth cones with area higher than the median (mean 0.5 ± 0.2 , $n = 57$, $P = 2e-5$) (Fig. 2e). Thus, larger growth cones balance a higher proportion of force locally.

Several possible physiological functions for neurite tension have been suggested^{1,3,11–19}. But what is the function of the additional force that does not contribute directly to resisting tension? Investigations of neuronal development *in vivo* have shown that growth cones within nerve tracts are thin and streamlined but pause in their migration and become complex and spread out when they reach ‘decision regions’⁴⁶. This could be interpreted as a mechanism for exploring space at a point where positional information has to be interpreted, guidance cues sensed, and directional changes executed. The large spread growth cones in the current data set show locally balanced forces that are not directly resisting tension and which might be involved in mechanosensing, exploring space for guidance cues, or initiating a change in growth trajectory.

Tension is stable during outgrowth. To investigate possible correlations between traction and outgrowth we sampled traction fields every 10 or 30 seconds in actively migrating growth cones. This timescale allowed us to resolve the transitions from one morphology and stress pattern to another, but also allowed us to track growth over tens of microns. Accompanying movies of strain energy density overlain on DIC images show that the growth cone and associated traction patterns are extremely dynamic during outgrowth (Fig. 3a,b). In contrast, total force and tension, quantities that are integrated over the entire growth cone, are surprisingly consistent throughout the period of observation (Fig. 3c,d). This observation is reminiscent of the pattern observed for DRG neurons²¹. For the population considered the standard deviation of the tension was 1.9 nN and the standard deviation of the total force was 5.3 nN. In comparison, the average standard deviation of the tension for individual growth cones over time was 0.8 nN, and the average standard deviation of the total force was 1.7 nN. Growth cones advanced steadily during observation and changes in growth rate were not associated with changes in force (Fig. 3c,d and Supplementary Fig. S3). This observation is similar to the findings of Koch et al.²¹. Further, average rates of advance do not depend strongly on tension, tension ratio, or area (Fig. 3e,f,g). It should be noted that three growth cones with tension >4 nN also showed the slowest growth (Fig. 3e). The sample size is insufficient to establish whether there is a correlation, but this point deserves further investigation.

The observed stability of tension over time suggests homeostatic maintenance within a narrow range. In fact, neurons have been shown to actively regulate tension to maintain a consistent value^{10,47}. The lack of correlation between tension and growth rate appears to contradict a body of evidence connecting externally applied tension with elongation^{15,47}. However, correlation between growth and

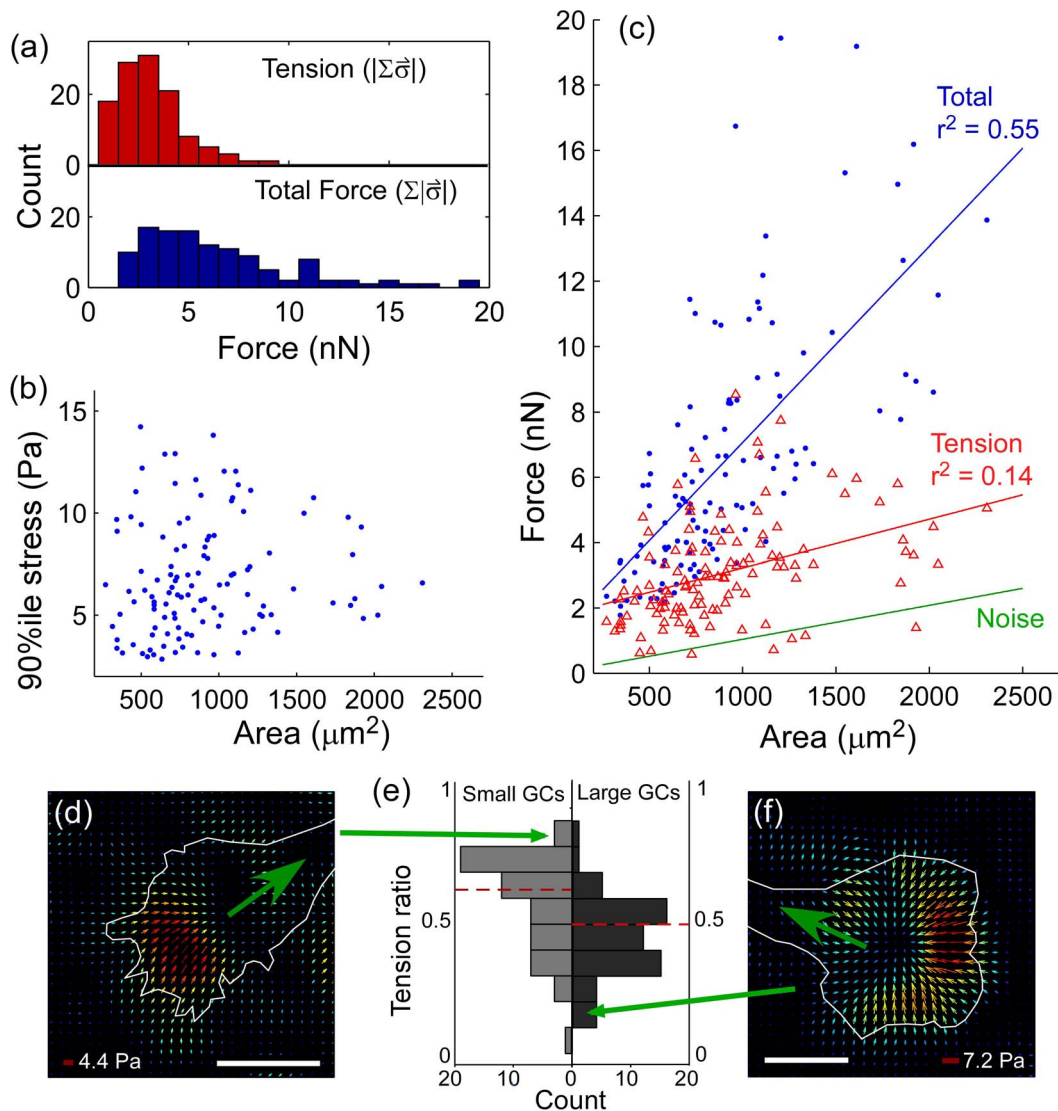


Figure 2 | Growth cone force scaling and local balance. (a) Histograms of tension and total force. (b) Plot of 90th percentile stress against growth cone area. (c) Plot of total force (blue symbols) and tension (red symbols) and expected total force value from noise only (green line) against growth cone area. (d) Example stress vector field of a growth cone illustrating a high tension ratio. Green arrow indicates direction of tension. (e) Histograms of the tension ratio for growth cones above (right) or below (left) the median area. (f) Example stress vector field of a growth cone illustrating a low tension ratio. Green arrow indicates direction of tension. For all plots $N = 117$ growth cones. Scale bars are $20 \mu\text{m}$.

internally generated tension, such as that imposed by growth cone tugging on the neurite, has never been clearly shown. Our data can be reconciled with the observations of tension-driven growth by a model in which the structure of the neurite continuously readjusts to maintain a set tension, elongating when the tension is greater than the set point and shortening when it is lower. Such a mechanism would require a tight feedback between growth cone advance, tension generation, and structural remodeling.

The independence of growth rate and growth cone size makes clear that the large, spread peripheral domain is not necessarily a ‘paused’ state, as suggested by *in vivo* studies⁴⁶. The lack of correlation between tension ratio and growth implies that stress field geometry does not limit growth rate. The fluctuations in tension (Fig. 2 c,d) appear smaller relative to the mean than those reported for DRG neurons, and the pattern contrasts sharply with the intermittent forces and movement observed in hippocampal neurons²¹. Both studies however demonstrate that a highly dynamic and rapidly turning over structure can generate a consistent total output.

Dynamic traction patterns balance a consistent tension. The steady tension must be maintained by a growth cone that is continually migrating and remodeling. Accompanying videos show that the force distribution changes rapidly as veils and filopodia protrude and retract (Supplementary Videos 1–4). How are the fluctuations in stress distribution coordinated to produce a consistent tension and total force? By examining the evolution of strain energy in different parts of a growth cone we find that traction dissipation in one area often corresponds to a rise in another, usually more distal, region (Fig. 4, Supplementary Fig. S4). Traction does not completely vanish in a region before starting to rise elsewhere, suggesting that a constant ‘load’ is being redistributed over the continuously remodeling growth cone structure.

Traction is rarely distributed evenly throughout the periphery and is often concentrated into one or more ‘hot spots’. We observe that as traction force shifts the central cytoplasmic domain bends towards areas of high force (Fig. 4a, Supplementary Videos 1–4). This is consistent with previous observations that a change in the direction of tension² or traction on ligand-coated beads can reorient neurites⁴⁸.

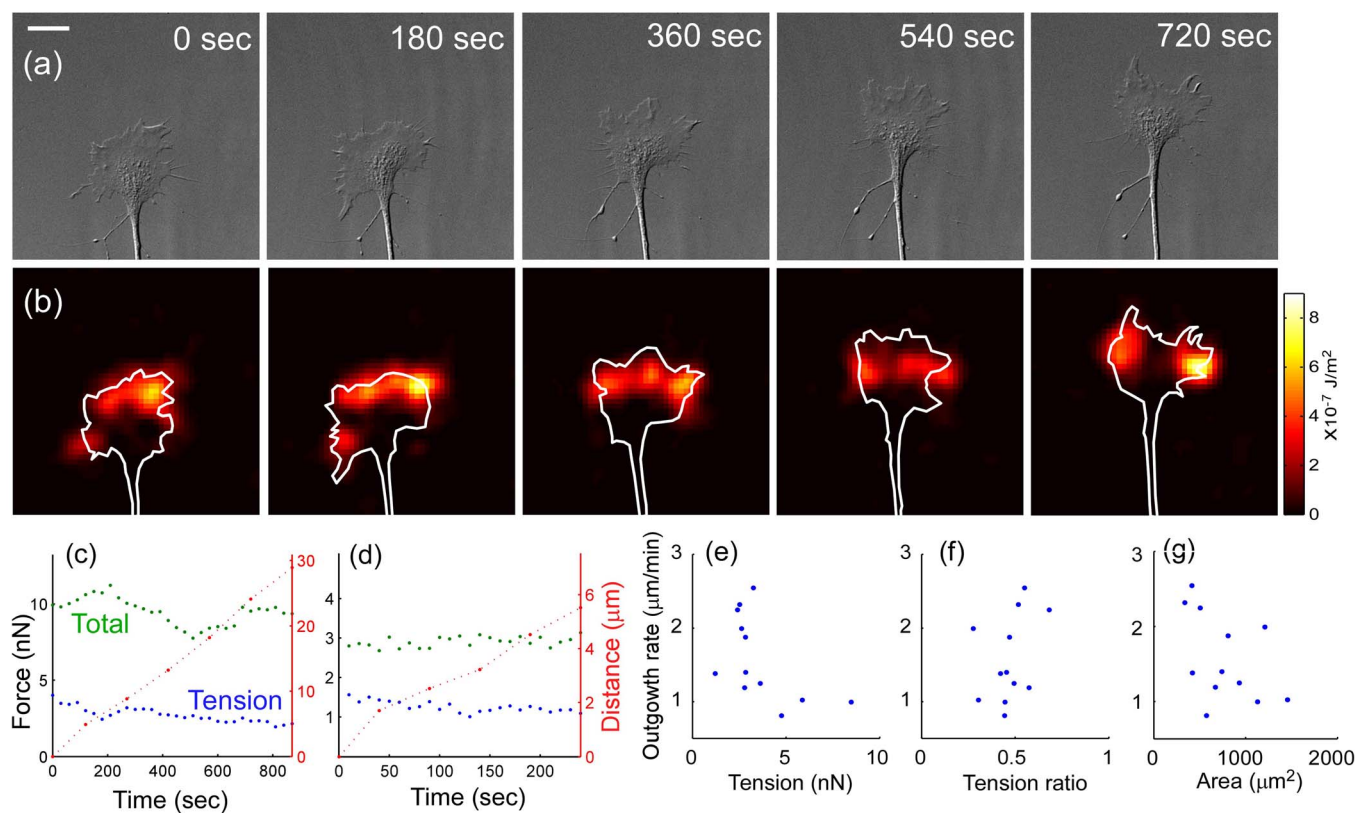


Figure 3 | Growth cone traction force is consistent during outgrowth. (a) DIC images and (b) strain energy density maps of a representative example growth cone advancing over 12 min. Scale bar is 20 μm . (c) Growth cone position (red line, right axis), tension (blue line, left axis), and total force (green line, left axis) over time for the growth cone in (a). (d) Growth cone position, tension, and total force for another representative growth cone. Growth rate vs. (e) tension, (f) tension ratio, (g) growth cone area ($N = 12$ growth cones).

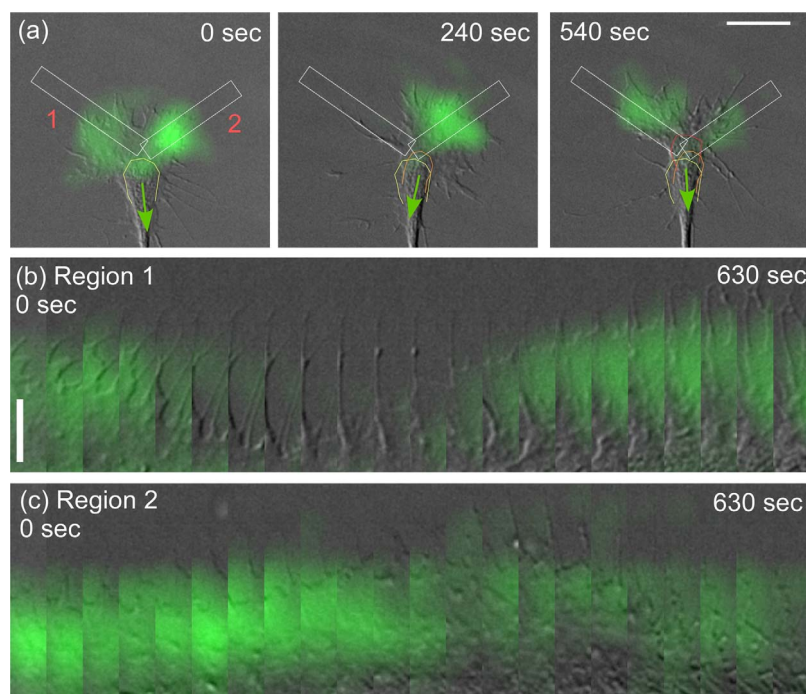


Figure 4 | Traction rises and falls in different areas of the growth cone during outgrowth. (a) Overlay of DIC and strain energy density (green) at three timepoints. Solid lines outline the central domain at 0 (yellow), 240 (orange), and 570 s (red). Scale bar is 20 μm . (b) Montage of growth sequence corresponding to region 1 in (a), with 30 s interval. Scale bar is 10 μm . (c) Montage corresponding to region 2, 30 s interval.



The direction of tension (green arrow, Fig. 4a, Supplementary Videos 1–4) is typically parallel to the direction of central domain pointing. The existence of neurite tension implies a mechanical connection between the peripheral domain and neurite shaft, and the association between peripheral traction, tension direction, and central movement (Fig. 4a) reveals tight mechanical coupling between of growth cone cytoplasmic domains during outgrowth and turning. This behavior of the central domain is reminiscent of the morphological changes that accompany the interaction of *Aplysia* growth cones with restrained ligand-coated beads or physiological substrates^{49–51}.

The rapid fluctuation of stress distribution is consistent with the current understanding of growth cone adhesion dynamics. Growth cones form highly dynamic structures called point contacts with a similar composition to the more stable focal adhesions of fibroblasts and other cells^{52,53}. These contacts are likely responsible for the mechanical coupling between cytoskeleton and substrate. Leading edge protrusions are stabilized by the formation of point contacts⁵² and modulation of contact dynamics may underly turning in response to guidance cues^{54,55}. Point contacts have an average lifetime of 2.2 minutes⁵², consistent with the time scale of appearance and dissipation of traction in different regions of the growth cone. According to a popular model of growth cone motility^{56,57}, traction between moving actin and substrate-anchored adhesions drives outgrowth by resisting retrograde flow and converting polymerization into leading edge protrusion. Examination of the accompanying movies shows that leading edge advance and appearance of traction are often out of phase (see Supplementary Video 2, 360–540 seconds and Supplementary Video 3, 390–600 seconds), suggesting that the forces measured here might not be directly involved in driving protrusion. Simultaneous visualization of adhesion, actin, and traction dynamics will clarify the connection between cell-substrate coupling and growth cone advance.

We propose a simple mechanical model for growth cone advance wherein the tension of the neurite shaft presents a constant load that is balanced by growth cone traction force (Fig. 5). This force is distributed among cell-substrate adhesions under the peripheral domain. When some adhesions break the force becomes redistributed among the existing adhesions. In our hypothesized model, this movement under constant load can be likened to a rock climber whose constant weight under gravity is continuously redistributed among shifting handholds and footholds. Thus growth may proceed by the formation of adhesions under the extending peripheral domain with subsequent loss of adhesions near the central domain and at the sides and rear of the growth cone. Our model also suggests

a mechanism by which off-axis traction force could initiate neurite turning. In response to guidance cues or substrate borders, the selective stabilization of adhesions on one side of the growth cone could lead to a reorganization of traction force, a shift in the direction of tension, and turning of the neurite toward the attractive cue (Fig. 5 a to b and c to d).

In conclusion, our measurements of growth cone traction force during neurite elongation have revealed that traction in the peripheral domain balances tension in the neurite shaft. This tension is independent of growth cone size while the total force increases with area. These data indicate that growth cones are mechanically integrated with the rest of the cell through neurite tension but can also be partly mechanically isolated when a portion of the force is balanced locally. The existence of partially isolated compartments may be a unique feature of neurons, necessary on account their extended morphology in which different parts of the cell must respond independently to their local environment. We also show that tension and total force, integral quantities describing growth cone force output, are consistent over time despite highly dynamic peripheral domain stress distributions.

The narrow range of neurite tensions within the population and the consistency of tension over time suggests that this might be a tightly regulated property. Identifying the feedback mechanisms and signaling pathways that contribute to force regulation will be an important subject of future study. Limits to tension may not arise from the growth cone itself, since large growth cones are clearly capable of generating tensions much larger than those measured, but might be a property of the neurite shaft. We propose that the growth cone moves under a constant load imposed by the neurite shaft. This load is continually redistributed among adhesions that form and break during advance.

Methods

Traction force substrate preparation. Traction force substrates were prepared by coating a glass coverslip with a highly elastic silicone gel as described⁵⁸, with the following modifications. One layer of fluorescent beads (100 nm or 40 nm yellow-green or red fluorescent carboxylate-modified microspheres, Invitrogen) at a 1 : 2000 volume ratio in 100% ethanol were deposited on the surface of an acid-washed coverslip by spin-coating at 2,000 RPM for 30 sec with a PWM32 spinner (Headway Research, Garland, TX). Silicone gel was prepared as a 1 : 1 weight ratio of CY52-276A and CY52-276B (Dow Corning Toray Silicones, Tokyo, Japan). The mixture was degassed for 10 minutes and applied to the coverslip by spin-coating for 30 seconds at 2,000 RPM. The film of silicone gel prepared in this manner was typically between 30 and 40 μm thick. The silicone was cured overnight at room temperature. Silicone gels prepared in this manner had a Young's modulus of 3 kPa.

After curing, fluorescent beads were deposited on the top surface of the silicone gel using a reaction of (3-Aminopropyl)triethoxysilane (APTES) and 1-ethyl-3-(3-

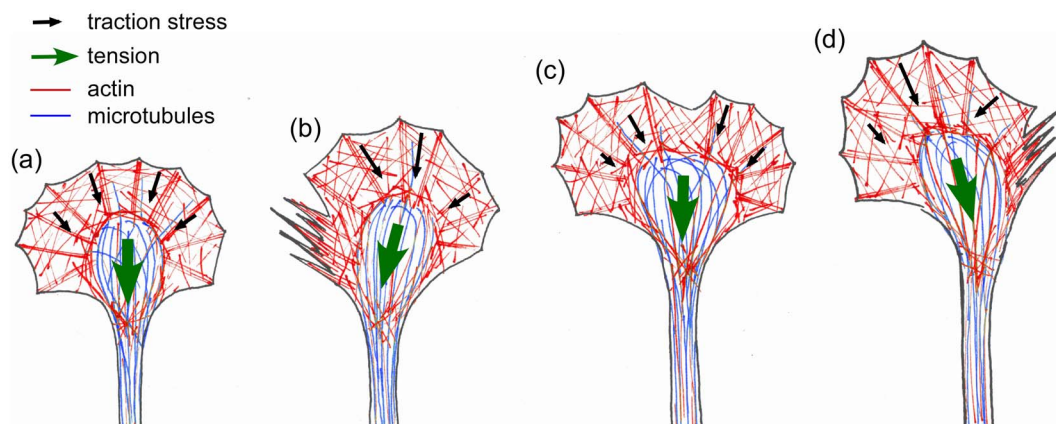


Figure 5 | Model for growth cone advance. Peripheral domain traction (red arrows) balances a constant load imposed by the neurite (orange arrow). When a portion of the growth cone retracts (a to b) the tension becomes redistributed among remaining points of attachment, accompanied by the movement of the central domain towards the region of higher force on the right. When a new region of peripheral domain advances (b to c) force is redistributed among the old and the newly formed adhesions. Detachment on right and advance of the peripheral domain on the left (c to d) again leads to the redistribution of traction and reorientation of the central domain.



dimethylaminopropyl)carbodiimide (EDC). APTES (Sigma-Aldrich, St. Louis, MO) was applied to the silicone gel surface by vapor deposition in a vacuum chamber for 4 hours. 1 mg/mL EDC (Sigma-Aldrich) was dissolved in 50 mM borate buffer and 100 nm green-yellow or red beads were added to a final dilution of 1:1,000 or 1:2,000 and sonicated with a VirSonic 100 probe sonicator (VerTis Co., Gardiner, NY). Silicone gel coated coverslips were then floated on top of this solution for 10–15 minutes.

Cell culture and media. Prior to plating bag cell neurons, vertebrate laminin (Sigma-Aldrich) diluted with *Aplysia* hemolymph to 50 $\mu\text{g}/\text{mL}$ was passively adsorbed onto the surface of TFM substrates for 1 hr at room temperature. Hemolymph was collected as previously described⁵⁹. Substrates were rinsed with L15 artificial sea water (ASW) (400 mM NaCl, 10 mM KCl, 15 mM HEPES, pH 7.8, 10 mM CaCl_2 , 55 mM MgCl_2 , and Phenol Red). Primary culture of *Aplysia* bag cell neurons was as previously described²⁹. Bag cells were grown overnight in L15-ASW either at room temperature or at 18°C prior to use in experiments. Experiments were performed at room temperature in L15-ASW supplemented with 0.5 mM vitamin E (Sigma-Aldrich) and 2 mg/ml carnosine (Sigma-Aldrich). Solutions containing Cytochalasin B (Sigma-Aldrich) and Jasplakinolide (Molecular Probes, Eugene, OR) were applied to cells using a homemade chamber in which a compartment containing the cells is separated from a solution exchange compartment by a Whatman Cyclo-pore track etched membrane with 5 μm pores (Whatman, Florham Park, NJ). This arrangement was necessary to prevent mechanical disturbance of the cells during solution exchange.

Image acquisition. Images were acquired on a Nikon TE2000E inverted microscope (Nikon, Melville, NY) and an Andor Revolution spinning disk confocal system (Andor, Belfast, UK) equipped with a CSU-X1 confocal head (Yokogawa, Tokyo, Japan) and a Andor iXon^{EM+}888 EM CCD camera. Confocal illumination was with 488 and 561 laser lines controlled with an Andor Laser Combiner. Emission wavelength was selected with bandpass filters from Chroma Technology (Bellows Falls, VT) mounted in a Sutter LB10W-2800 filter wheel. Transillumination was with a halogen lamp and SmartShutter (Sutter Instruments, Novato, CA). All hardware and image acquisition were controlled with μ -Manager software⁶⁰. Objectives used were Plan Apo VC 100 \times /1.4 numerical aperture (NA), phase contrast Plan Apo 100 \times /1.45 NA, Plan Apo 60 \times /1.4 NA, and phase contrast Plan Apo 60 \times /1.4 NA (Nikon).

TFM data consisted of single fields at single time points or a single field imaged at multiple time points. For each field a phase contrast or DIC image was acquired of the growth cone, then a confocal image was acquired of the upper layer of fluorescent beads. The growth cone was centered in the field of view such that bead displacements would be expected to decrease to zero at the edges. For all TFM experiments an unstressed reference image was required to calculate absolute stress magnitudes. Accordingly, after the experiment, chambers were perfused with 1% Triton X-100 (Sigma-Aldrich) in ASW to dissolve cells and relax the stress exerted by the cells on the substrate. A confocal z-stack of the beads was then acquired for every field of interest.

Calculation of traction fields, strain energy, and internal stress. All TFM data was analyzed in MATLAB (MathWorks) and imaging processing was with either MATLAB or ImageJ⁶¹. Bead positions were found using MATLAB's centroid analysis⁶² from either single confocal images or average intensity projections of z-stacks. The deformation of the substrate, $u_i(\mathbf{r})$, was found by calculating the distance between centroids of stressed images and the unstressed reference image⁶³. Linear elasticity theory relates the traction stress to the deformation in Fourier space by $\sigma_{iz}(\mathbf{k}, h_s) = Q_{ij}(\mathbf{k}, h_s)u_j(\mathbf{k})$, where \mathbf{k} is the in-plane wave vector and h_s is the thickness of the substrate. $\sigma_{iz}(\mathbf{k}, h_s)$ and $u_j(\mathbf{k})$ are the Fourier transforms of the traction stress and bead displacements, respectively. The tensor Q is dependent on the elastic properties of the silicone gel, the wave vector, and h_s ^{64,65}. The strain energy density, a scalar quantity equivalent to the energy per unit area expended by the cell to deform the substrate, was calculated as $w(\mathbf{r}) = \frac{1}{2} \sigma_{iz}(\mathbf{r}, h_s)u_i(\mathbf{r})$ ⁶⁶. Tension was calculated as the magnitude of the vector sum of stresses over the area of the growth cone, $\left| \int dA (\sigma_{xz}\hat{x} + \sigma_{yz}\hat{y}) \right|$, and the total force was calculated as the scalar sum of stress magnitudes over the area of the growth cone, $\int dA |\sigma_{xz}\hat{x} + \sigma_{yz}\hat{y}|$, where \hat{x} and \hat{y} are unit vectors. Noise was estimated by finding the average stress magnitude, $\left(\int dA |\sigma_{xz}\hat{x} + \sigma_{yz}\hat{y}| \right) / A$, for regions outside the growth cone in a subset of traction force maps.

Linescans were made by drawing a line from the leading edge, through the region of highest strain energy, and into the neck of the growth cone. For strain energy density traces, the strain energy density map was sampled at regular intervals along the line. Stress along the line was found by projecting adjacent stress vectors onto the line. Internal stress along the line was estimated using $\sigma_{xx} = \int dx(\sigma_{xz}/h)$ as described^{39,40}. The thickness of the growth cone, h , was taken to be 180 nm in the peripheral domain and 1300 nm in the central domain⁶⁷. The internal stress calculation assumes that all stress is oriented along the line and the gradient of the stress perpendicular to the line is small. This is a good approximation of our data since the linescan is parallel to the direction of stress and through a maximum. Growth was measured from DIC images as displacement of the growth cone's central domain along the inferred growth axis, sampled every 50 or 150 seconds.

Statistical analysis. All statistical analyses were performed in MATLAB. p values were determined with a Wilcoxon paired-sample test for comparison of drug treatments to control, and with a two-sided Wilcoxon rank sum test for comparison of tension ratios. Statistical significance was defined as $p < 0.05$.

- Smith, D. H. Stretch growth of integrated axon tracts: Extremes and exploitations. *Prog. Neurobiol.* **89**, 231–239 (2009).
- Bray, D. Mechanical tension produced by nerve cells in tissue culture. *J. Cell Sci.* **37**, 391–410 (1979).
- Lamoureux, P., Buxbaum, R. E. & Heidemann, S. R. Direct evidence that growth cones pull. *Nature* **340**, 159–162 (1989).
- Dennerll, T. J., Joshi, H. C., Steel, V. L., Buxbaum, R. E. & Heidemann, S. R. Tension and compression in the cytoskeleton of PC-12 neurites. II: quantitative measurements. *J. Cell Biol.* **107**, 665–674 (1988).
- Bernal, R., Pullarkat, P. A. & Melo, F. Mechanical properties of axons. *Phys. Rev. Lett.* **99**, 018301 (2007).
- Bernal, R., Melo, F. & Pullarkat, P. A. Drag force as a tool to test the active mechanical response of PC12 neurites. *Biophys. J.* **98**, 515–523 (2010).
- Ahmad, F. J. *et al.* Motor proteins regulate force interactions between microtubules and microfilaments in the axon. *Nat. Cell Biol.* **2**, 276–280 (2000).
- Condic, M. L. & Bentley, D. Removal of the basal lamina in vivo reveals growth cone-basal lamina adhesive interactions and axonal tension in grasshopper embryos. *J. Neurosci.* **9**, 2678–2686 (1989).
- Condron, B. G. & Zinn, K. Regulated neurite tension as a mechanism for determination of neuronal arbor geometries in vivo. *Curr. Biol.* **7**, 813–816 (1997).
- Rajagopalan, J., Tofangchi, A. & A Saif, M. T. *Drosophila* neurons actively regulate axonal tension in vivo. *Biophys. J.* **99**, 3208–3215 (2010).
- Heidemann, S. R., Lamoureux, P. & Buxbaum, R. E. Cyto mechanics of axonal development. *Cell Biochem. Biophys.* **27**, 135–155 (1997).
- Weiss, P. Nerve pattern: the mechanics of nerve growth. In *Growth, Third Growth Symposium* 163–203 (1941).
- Pfister, B. J., Iwata, A., Meaney, D. F. & Smith, D. H. Extreme stretch growth of integrated axons. *J. Neurosci.* **24**, 7978–7983 (2004).
- Bray, D. Axonal growth in response to experimentally applied mechanical tension. *Dev. Biol.* **102**, 379–389 (1984).
- Zheng, J. *et al.* Tensile regulation of axonal elongation and initiation. *J. Neurosci.* **11**, 1117–1125 (1991).
- Lamoureux, P., Ruthel, G., Buxbaum, R. E. & Heidemann, S. R. Mechanical tension can specify axonal fate in hippocampal neurons. *J. Cell Biol.* **159**, 499–508 (2002).
- Anava, S., Greenbaum, A., Ben Jacob, E., Hanein, Y. & Ayali, A. The regulative role of neurite mechanical tension in network development. *Biophys. J.* **96**, 1661–1670 (2009).
- Van Essen, D. C. A tension-based theory of morphogenesis and compact wiring in the central nervous system. *Nature* **385**, 313–318 (1997).
- Hilgetag, C. C. & Barbas, H. Role of mechanical factors in the morphology of the primate cerebral cortex. *PLoS Comput. Biol.* **2**, e22 (2006).
- Betz, T., Koch, D., Lu, Y.-B., Franze, K. & Ks, J. A. Growth cones as soft and weak force generators. *Proc. Natl. Acad. Sci.* **108**, 13420–13425 (2011).
- Koch, D., Rosoff, W. J., Jiang, J., Geller, H. M. & Urbach, J. S. Strength in the periphery: growth cone biomechanics and substrate rigidity response in peripheral and central nervous system neurons. *Biophys. J.* **102**, 452–460 (2012).
- Chan, C. E. & Odde, D. J. Traction dynamics of filopodia on compliant substrates. *Science* **322**, 1687–1691 (2008).
- Bridgman, P. C., Dave, S., Asnes, C. F., Tullio, A. N. & Adelstein, R. S. Myosin IIB is required for growth cone motility. *J. Neurosci.* **21**, 6159–6169 (2001).
- Toriyama, M., Kozawa, S., Sakumura, Y. & Inagaki, N. Conversion of a signal into forces for axon outgrowth through Pak1-mediated shootin1 phosphorylation. *Curr. Biol.* **23**, 529–534 (2013).
- Franze, K. *et al.* Neurite branch retraction is caused by a threshold-dependent mechanical impact. *Biophys. J.* **97**, 1883–1890 (2009).
- Schwarz, U. & Gardel, M. United we stand: integrating the actin cytoskeleton and cell-matrix adhesions in cellular mechanotransduction. *J. Cell Sci.* **125**, 3051–3060 (2012).
- Kraning-Rush, C., Carey, S., Califano, J. & Reinhart-King, C. Chapter 6 - quantifying traction stresses in adherent cells. In Asthagiri, A. R. & Arkin, A. P. (ed.) *Methods Cell Biol.* vol. 110, 139–178 (Academic Press, 2012).
- Gardel, M. L., Schneider, I. C., Aratyn-Schaus, Y. & Waterman, C. M. Mechanical integration of actin and adhesion dynamics in cell migration. *Annu. Rev. Cell Dev. Biol.* **26**, 315–333 (2010).
- Forscher, P., Kaczmarek, L. K., Buchanan, J. A. & Smith, S. J. Cyclic AMP induces changes in distribution and transport of organelles within growth cones of *Aplysia* bag cell neurons. *J. Neurosci.* **7**, 3600–3611 (1987).
- Lewis, A. K. & Bridgman, P. C. Nerve growth cone lamellipodia contain two populations of actin filaments that differ in organization and polarity. *J. Cell Biol.* **119**, 1219–1243 (1992).
- Dent, E. W., Gupton, S. L. & Gertler, F. B. The growth cone cytoskeleton in axon outgrowth and guidance. *Cold Spring Harb. Perspect. Biol.* **3**, 1–39 (2011).
- Schaefer, A. W., Kabir, N. & Forscher, P. Filopodia and actin arcs guide the assembly and transport of two populations of microtubules with unique dynamic parameters in neuronal growth cones. *J. Cell Biol.* **158**, 139–152 (2002).



33. Zhang, X.-F., Schaefer, A. W., Burnette, D. T., Schoonderwoert, V. T. & Forscher, P. Rho-dependent contractile responses in the neuronal growth cone are independent of classical peripheral retrograde actin flow. *Neuron* **40**, 931–944 (2003).
34. Burnette, D. T. *et al.* Myosin II activity facilitates microtubule bundling in the neuronal growth cone neck. *Dev. Cell* **15**, 163–169 (2008).
35. Forscher, P. & Smith, S. J. Actions of cytochalasins on the organization of actin filaments and microtubules in a neuronal growth cone. *J. Cell Biol.* **107**, 1505–1516 (1988).
36. Van Goor, D., Hyland, C., Schaefer, A. W. & Forscher, P. The role of actin turnover in retrograde actin network flow in neuronal growth cones. *PLoS ONE* **7**, e30959 (2012).
37. Lin, C. H., Espreafico, E. M., Mooseker, M. S. & Forscher, P. Myosin drives retrograde f-actin flow in neuronal growth cones. *Neuron* **16**, 769–782 (1996).
38. Medeiros, N. A., Burnette, D. T. & Forscher, P. Myosin II functions in actin-bundle turnover in neuronal growth cones. *Nat. Cell Biol.* **8**, 215–226 (2006).
39. Trepast, X. *et al.* Physical forces during collective cell migration. *Nat. Phys.* **5**, 426–430 (2009).
40. Xu, Y., German, G. K., Mertz, A. F. & Dufresne, E. R. Imaging stress and strain in the fracture of drying colloidal films. *Soft Matter* **9**, 3735–3740 (2013).
41. Legant, W. R. *et al.* Multidimensional traction force microscopy reveals out-of-plane rotational moments about focal adhesions. *Proc. Natl. Acad. Sci.* **110**, 881–886 (2013).
42. Schwarz Henriques, S., Sandmann, R., Strate, A. & Köster, S. Force field evolution during human blood platelet activation. *J. Cell Sci.* **125**, 3914–3920 (2012).
43. Fournier, M. F., Sauser, R., Ambrosi, D., Meister, J.-J. & Verkhovsky, A. B. Force transmission in migrating cells. *J. Cell Biol.* **188**, 287–297 (2010).
44. Maruthamuthu, V., Sabass, B., Schwarz, U. S. & Gardel, M. L. Cell-ECM traction force modulates endogenous tension at cell-cell contacts. *Proc. Natl. Acad. Sci.* **108**, 4708–4713 (2011).
45. Liu, Z. *et al.* Mechanical tugging force regulates the size of cell-cell junctions. *Proc. Natl. Acad. Sci.* **107**, 9944–9949 (2010).
46. Mason, C. & Erskine, L. Growth cone form, behavior, and interactions in vivo: Retinal axon pathfinding as a model. *J. Neurobiol.* **44**, 260–270 (2000).
47. Dennerll, T. J., Lamoureaux, P., Buxbaum, R. E. & Heidemann, S. R. The cytomechanics of axonal elongation and retraction. *J. Cell Biol.* **109**, 3073–3083 (1989).
48. Moore, S. W., Biais, N. & Sheetz, M. P. Traction on immobilized netrin-1 is sufficient to reorient axons. *Science* **325**, 166 (2009).
49. Schaefer, A. W. *et al.* Coordination of actin filament and microtubule dynamics during neurite outgrowth. *Dev. Cell* **15**, 146–162 (2008).
50. Suter, D. M. & Forscher, P. Transmission of growth cone traction force through apCAM-cytoskeletal linkages is regulated by Src family tyrosine kinase activity. *J. Cell Biol.* **155**, 427–438 (2001).
51. Lin, C. H. & Forscher, P. Cytoskeletal remodeling during growth cone-target interactions. *J. Cell Biol.* **121**, 1369–1383 (1993).
52. Woo, S. & Gomez, T. M. Rac1 and RhoA promote neurite outgrowth through formation and stabilization of growth cone point contacts. *J. Neurosci.* **26**, 1418–1428 (2006).
53. Gomez, T. M., Roche, F. K. & Letourneau, P. C. Chick sensory neuronal growth cones distinguish fibronectin from laminin by making substratum contacts that resemble focal contacts. *J. Neurobiol.* **29**, 18–34 (1996).
54. Robles, E. & Gomez, T. M. Focal adhesion kinase signaling at sites of integrin-mediated adhesion controls axon pathfinding. *Nat. Neurosci.* **9**, 1274–1283 (2006).
55. Myers, J. P., Santiago-Medina, M. & Gomez, T. M. Regulation of axonal outgrowth and pathfinding by integrin-ECM interactions. *Dev. Neurobiol.* **71**, 901–923 (2011).
56. Lowery, L. A. & Van Vactor, D. The trip of the tip: understanding the growth cone machinery. *Nat. Rev. Mol. Cell Biol.* **10**, 332–343 (2009).
57. Suter, D. M. & Forscher, P. Substrate-cytoskeletal coupling as a mechanism for the regulation of growth cone motility and guidance. *J. Neurobiol.* **44**, 97–113 (2000).
58. Mertz, A. F. *et al.* Cadherin-based intercellular adhesions organize epithelial cell-matrix traction forces. *Proc. Natl. Acad. Sci.* **110**, 842–847 (2013).
59. Schacher, S. & Proshansky, E. Neurite regeneration by *Aplysia* neurons in dissociated cell culture: modulation by aplysia hemolymph and the presence of the initial axonal segment. *J. Neurosci.* **3**, 2403–2413 (1983).
60. Edelstein, A., Amodaj, N., Hoover, K., Vale, R. & Stuurman, N. *Curr. Protoc. Mol. Biol.* chap. Computer Control of Microscopes Using μ Manager (John Wiley and Sons, Hoboken NJ, 2010).
61. Schneider, C. A., Rasband, W. S. & Eliceiri, K. W. NIH image to ImageJ: 25 years of image analysis. *Nat. Methods* **9**, 671–675 (2012).
62. Crocker, J. C. & Grier, D. G. Methods of digital video microscopy for colloidal studies. *J. Colloid Interface Sci.* **179**, 298–310 (1996).
63. Blair, D. L. & Dufresne, E. R. The matlab particle tracking code repository. [Http://physics.georgetown.edu/matlab/](http://physics.georgetown.edu/matlab/).
64. Xu, Y. *et al.* Imaging in-plane and normal stresses near an interface crack using traction force microscopy. *Proc. Natl. Acad. Sci.* **107**, 14964–14967 (2010).
65. Del Alamo, J. C. *et al.* Spatio-temporal analysis of eukaryotic cell motility by improved force cytometry. *Proc. Natl. Acad. Sci.* **104**, 13343–13348 (2007).
66. Butler, J. P., Tolić-Norrelykke, I. M., Fabry, B. & Fredberg, J. J. Traction fields, moments, and strain energy that cells exert on their surroundings. *Am. J. Physiol. Cell Physiol.* **282**, C595–605 (2002).
67. Xiong, Y., Lee, A. C., Suter, D. M. & Lee, G. U. Topography and nanomechanics of live neuronal growth cones analyzed by atomic force microscopy. *Biophys. J.* **96**, 5060–5072 (2009).

Acknowledgments

We are grateful to Jeffery S. Urbach (Georgetown University) for helpful discussions. This work was supported by National Science Foundation Graduate Research Fellowships (to C.H. and A.F.M.), National Institutes of Health Grants RO1-NS28695 and RO1-NS051786 (to P.F.), and National Science Foundation Grant DBI-0619674 (to E.R.D. and P.F.).

Author contributions

C.H., A.F.M., P.F. and E.R.D. designed research and wrote the paper, C.H. performed experiments, analyzed data and prepared figures.

Additional information

Supplementary information accompanies this paper at <http://www.nature.com/scientificreports>

Competing financial interests: The authors declare no competing financial interests.

How to cite this article: Hyland, C., Mertz, A.F., Forscher, P. & Dufresne, E. Dynamic peripheral traction forces balance stable neurite tension in regenerating *Aplysia* bag cell neurons. *Sci. Rep.* **4**, 4961; DOI:10.1038/srep04961 (2014).



This work is licensed under a Creative Commons Attribution-NonCommercial-NoDerivs 3.0 Unported License. The images in this article are included in the article's Creative Commons license, unless indicated otherwise in the image credit; if the image is not included under the Creative Commons license, users will need to obtain permission from the license holder in order to reproduce the image. To view a copy of this license, visit <http://creativecommons.org/licenses/by-nc-nd/3.0/>